JOURNAL OF NATURAL REMEDIES
DOI: 10.18311/jnr/2025/50710

SHORT COMMUNICATION

Exploring the Anti-psoriatic Potential of Bioactive Compounds from *Rhinacanthus nasutus* and *Solanum nigrum* Leaves through Molecular Docking and Dynamics Simulation Studies

Vaheeda Rahman and A. Vijayalakshmi*

Department of Pharmacognosy, Vels Institute of Science, Technology and Advanced Studies, Pallavaram - 600117, Chennai, Tamil Nadu, India; avijibaskaran@gmail.com

Abstract

Background: Ethnomedicinal plants have long been recognized for their therapeutic potential in managing inflammatory and skin-related disorders, with several species demonstrating promising bioactivity through both traditional use and modern pharmacological investigations. **Aim:** To investigate the anti-psoriatic potential of bioactive compounds from *Rhinacanthus nasutus* and *Solanum nigrum* leaves through molecular docking and dynamics simulation studies. **Methods:** We investigated two ethnomedicinal plants, *R. nasutus* and *S. nigrum*, which have been used traditionally for healing skin diseases that mimic psoriasis. A parallel *in silico* study was performed for assessing the activity of their bioactive molecules (Rhinacanthin D and Trihydroxyflavone) on molecular targets linked with psoriasis such as Tyk2, PDE4D and S1P1 Receptor (S1P1R). Molecular docking studies were conducted using Auto Dock Vina, followed by 100 ns molecular dynamics simulations using GROMACS to verify the stability of ligand-protein complexes. **Results:** Analysis of the binding energies indicated favorable binding for both compounds, with rhinacanthin D showing high favorable interactions with these key inflammatory molecules. Molecular dynamics simulations confirmed the stability of the ligand-protein complexes, as evidenced by Root-Mean-Square Deviation (RMSD), Fluctuation (RMSF), and hydrogen bond occupancy analyses. The Binding Free Energy (BFE) results further corroborated the strength of interaction, especially for rhinacanthin D-included complexes. **Conclusion:** The findings are indicative of the potential use of *R. nasutus* and *S. nigrum* compounds as lead compounds against anti-psoriatic agents, thus providing a scientific foundation for the traditional use of these plants for treatment of psoriasis. However, comprehensive *in vitro* and *in vivo* studies are essential to validate these computational insights and translate them into viable therapeutic applications.

Major Findings: Rhinacanthin D demonstrated strong and stable interactions with key psoriasis-related targets (Tyk2, PDE4D, and S1P1R) across docking and molecular dynamics analyses. The computational outcomes support its potential as a lead anti-psoriatic compound, warranting further experimental validation.

Keywords: Ethnomedicinal Plants, PDE4D, Psoriasis, *R. nasutus*, *S. nigrum*, Rhinacanthin D, S1P1 Receptor, Trihydroxyflavone, Tyk2

1. Introduction

Psoriasis is a chronic immune-mediated skin disorder affecting 2-3% of the global population[1]. It is characterized by erythematous, scaly plaques caused by keratinocyte hyperproliferation, angiogenesis, and infiltration of immune cells such as Th17 cells and neutrophils[2]. The disease is driven by dysregulated cytokine networks, particularly TNF-α, IL-17A, and IL-23, which activate key inflammatory pathways including NF-κB, MAPK, and JAK-STAT[3,4]. Among molecular targets, phosphodiesterase 4D (PDE4D; PDB ID: 5K32) regulates intracellular cAMP, with reduced cAMP linked to enhanced cytokine release[5]. Tyrosine

*Author for correspondence

Article Received on: 20.07.2025 Revised on: 19.09.2025 Accepted on: 12.11.2025

kinase 2 (TYK2; PDB ID: 4GIH) is a critical mediator of IL-12/IL-23 signalling and Th1/Th17 differentiation[6], while Sphingosine-1-Phosphate Receptor 1 (S1P1R; PDB ID: 3V2W) controls immune cell trafficking and skin immune homeostasis[7]. Although biologics and small-molecule inhibitors targeting these pathways exist, their limitations-such as high cost, adverse systemic effects, and resistance development-necessitate alternative therapies[8]. These obstacles have led to the research focus on plant-derived compounds that provide multi-targeted effects and could have less detrimental effects and more patient's compliance. Various ethnomedicinal plants like *R. nasutus* and *S. nigrum* were in use traditionally to cure inflammatory skin diseases[9,10]. *R. nasutus* has the naphthoquinone rhinacanthin D and rhinacanthin C that has strong anti-inflammatory, antioxidant activities through blocking NF-κB and MAPK signaling pathways[11]. Trihydroxyflavone is the major constituents of *S. nigrum* which are both immunomodulatory and free radical scavenger[12]. These phytoconstituents were previously isolated by preparative HPLC and were further purified for the chromatographic purity before using in computational studies[13]. In this study, we use an *in silico* drug discovery strategy to explore the molecular binding of these phytoconstituents towards psoriasis-related targets (PDE4D, TYK2, and S1P1R). Ligands were obtained from PubChem, optimized by DFT and docked against using AutoDock Vina. Pharmacokinetic profile and drug-likeness properties were predicted by Swiss ADME according to the Lipinski's, Veber's, and Ghose's rules[14]. The ranked complexes were subjected to 100 ns MD simulations by using GROMACS and further impose MM-PBSA-based free energy analysis[15]. This *in silico* method emphasises the importance of *R. nasutus* and *S. nigrum* phytoconstituents in the treatment of psoriasis, and provides leads that can be further developed into natural, safe and multi-targeted drugs against psoriasis.

2. Materials and Methods

2.1 Plant Material and Extraction

The leaves of both *R. nasutus* and *S. nigrum* were collected, authenticated, shade-dried, and ground into powder. Each powdered sample (200 g) was subjected to Soxhlet extraction using 70% ethanol (v/v) as the solvent[16].

2.2 Preparative HPLC and Identification

The crude extracts underwent chromatographic separation on a C18 column using a gradient of acetonitrile and water containing 0.1% formic acid. Detection was set at 254 nm[17].

2.3 Pharmacokinetic Screening

The Swiss ADME tool was used to evaluate a compound's ADME properties alongside drug-likeness. These included Lipinski's Rule of Five as well as Veber's criteria and Ghose filters which assessed the compound's oral bioavailability potential and its suitability as a drug candidate[18].

2.4 Ligand Preparation

Structures of the identified compounds were downloaded from PubChem and optimized through geometry DFT calculations at B3LYP/6-31G(d,p) basis set. Docking simulations were performed with the optimized ligands[19].

2.5 Protein Target Preparation

Psoriasis-related proteins were retrieved from RCSB PDB: PDE4D (5K32), TYK2 (4GIH) and S1P1R (3V2W). Structures were processed through hydration shell removal, hydrogen addition, and charge assignment with AutoDock Tools[20-25].

2.6 Molecular Docking

Docking studies were carried out using AutoDock Vina, with the grid box centered on the co-crystallized ligand binding site of each protein to ensure docking within the biologically relevant active pocket. The grid center coordinates were set at X = 14.252, Y = 45.877, Z = 11.980 for PDE4D (PDB ID: 5K32), X = -7.964, Y = -8.699, Z = -16.866 for TYK2 (PDB ID: 4GIH), and X = 5.792, Y = 17.624, Z = -8.937 for S1P1R (PDB ID: 3V2W). The grid box dimensions were defined as [XX × YY × ZZ Å] with a spacing of 0.375 Å, large enough to encompass the active site region and allow conformational flexibility of ligands. These coordinates were derived from the crystallographic ligand position in the respective PDB structures, following established docking protocols[26,27].

2.7 Molecular Dynamics Simulations

Molecular Dynamics (MD) simulations were performed using GROMACS version 2022.2. Ligand-protein

complexes were built and saved in PDB format using PyMOL. Protein topology files were generated with the pdb2gmx module employing the CHARMM27 force field, while ligand topologies were obtained from the SwissParam server. Each complex was solvated in a cubic TIP3P water box with a minimum distance of 1.0 nm between the protein surface and the box edge, and periodic boundary conditions were applied in all directions. Na^+ counter ions were added to neutralize the system. Energy minimisation was conducted using the steepest descent algorithm (50,000 steps). Equilibration was carried out in 2 phases: A 100 ps NVT ensemble at 300 K, followed by a 100 ps NPT ensemble. Temperature and pressure were maintained using the Berendsen thermostat (τ = 0.1 ps) and Berendsen barostat (τ = 2 ps), respectively, with independent coupling of protein, ligand, water, and ions. The LINCS algorithm was used to constrain all bond lengths. Production MD simulations were then performed for 100 ns under NPT conditions at 300 K and 1 bar, with pressure coupling applied at a time constant of 1 ps. Trajectories were visualized in VMD 1.9.2, while post-simulation analyses-including RMSD, RMSF, radius of gyration, and hydrogen bond occupancy-were

Table 1. Identified phytoconstituents from *R. nasutus* and *S. nigrum*

Compound Name	Source Plant	Structure
Rhinacanthin D	*R. nasutus*	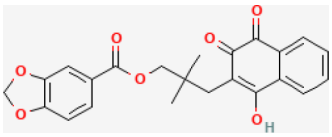
Rhinacanthin C	*R. nasutus*	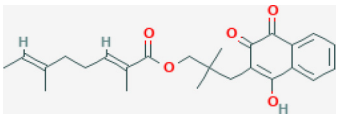
Trihydroxy flavone	*S. nigrum*	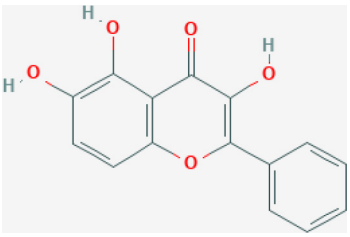

Table 2. ADMET and drug-likeness properties of selected phytoconstituents

Property	Rhinacanthin D	Trihydroxyflavone	Rhinacanthin C
Molecular weight (g/mol)	408.40	270.2	410.50
H-bond donors (≤5)	1	3	1
H-bond acceptors (≤10)	7	5	5
LogP (Lipophilicity)	3.72	2.58	5.37
TPSA (≤140 Å^2)	99.13	90.90	80.67
Rotatable bonds (≤10)	6	1	9
GI absorption	High	High	-
BBB permeability	No	No	-
CYP inhibition potential	No major inhibition	No major inhibition	-
Lipinski rule violations	0	0	1
Veber's rule (TPSA ≤140 and RB ≤10)	Yes	Yes	-
Bioavailability score	0.56	0.55	-

conducted using HeroMDAnalysis and Xmgrace 5.1.25[28-30].

3. Results

The key phytoconstituents obtained from *R. nasutus* and *S. nigrum* using preparative HPLC are shown in Table 1. From *R. nasutus*, we isolated the naphthoquinone derivative rhinacanthin D which is well-studied for its anti-inflammatory activity. From *S. nigrum*, we identified trihydroxyflavone which is them flavonoid and a steroidal alkaloid, respectively. We chose these compounds for *in silico* screening due to their documented ethnopharmacological uses and phytochemical profiles. Below are their chemical structures.

The ADMET and drug-likeness characteristics of rhinacanthin D, trihydroxyflavone, and rhinacanthin C were predicted using SwissADME and are summarized in Table 2. Rhinacanthin D and trihydroxyflavone complied with both Lipinski's Rule of Five and Veber's criteria, indicating favorable oral bioavailability. However, rhinacanthin C violated Lipinski's rule due to its high lipophilicity (LogP> 5). Both rhinacanthin D and trihydroxyflavone exhibited strong predicted gastrointestinal absorption, moderate polarity, and negligible CYP inhibition, establishing their metabolic safety potential.

Molecular docking studies indicated that for all 3 psoriasis-associated targets, Rhinacanthin D not only outperformed the reference standards but had remarkably higher binding affinity as represented in Table 3. For instance, rhinacanthin D's binding energy with PDE4D (5K32) was -9.5 kcal/mol (Table 4, Figure 1) which surpassed that of Apremilast, a clinically used PDE4 inhibitor for psoriasis, whose binding energy is -9.0 kcal/mol. This indicates the possibility for the compound to inhibit cAMP degradation and exert anti-inflammatory action downstream.

For TYK2 (4GIH) also, rhinacanthin D demonstrated more favorable docking energy of -9.3 kcal/mol (Table 5, Figure 2) compared to Deucravacitinib's binding energy of -8.0 kcal/mol, signifying the compound's possible effectiveness in blocking the JAK-STAT driven IL-23/Th17 signaling pathway important in psoriasis. Notably, another compound trihydroxyflavone demonstrated significant docking interaction of -8.6 kcal/mol toward the same enzyme, albeit less potent than deucravacitin.

Table 3. Docking scores (kcal/mol) of standard drugs and phytoconstituents against psoriasis-related targets

Compound	PDE4D (5K32)	TYK2 (4GIH)	S1P1R (3V2W)
Standards			
Apremilast	-9.0	-	-
Deucravacitinib	-	-8.0	
Ponesimod	-	-	-6.0
Ligands			
Rhinacanthin D	-9.5	-9.3	-8.7
Trihydroxyflavone	-8.6	-8.6	-9.1

Table 4. Docking scores, amino acid interactions, and hydrogen bonds of rhinacanthin D, trihydroxyflavone, and apremilast with 5K32

S. No	Compound	Docking Score	Amino Acid Interaction	Conventional Hydrogen Interaction
1	Rhinacanthin D	-9.5	PHE A:372, TYR A:159, PHE A:340, ILE A:336, LEU A:319, HIS A:204, HIS A:160, MET A:273, THR A:271, GLU A:230, SER A:208, LEU A:229, ASN A:209, ASN A:321, TRP A:332, PRO A:322, THR A:333, TYR A:329, GLN A:369, ASP A:272, SER A:274, LEU A:319, TYR A:159, LEU A:319.	MET A:273 THR A:271
2	Trihydroxyflavone	-8.6	PHE A:340, ILE A:336, PHE A:372, GLN A:369, HIS A:160, TYR A:159, LEU A:319, ASP A:318, ASN A:321, PRO A:322, HIS A:164, ASP A:201, HIS A:200	TYR A:159, ASP A:318.
3	Apremilast	-9.0	PHE A:340, PHE A:372, ILE A:336, VAL A:207, HIS A:160, MET A:273, HIS A:164, ASP A:201, ASP A:318, LEU A:319, ASN A:321, TRP A:332, THR A:333, TYR A:329, PRO A:322, GLN A:369, GLN A:343, GLU A:339, GLY A:206, SER A:208, HIS A:204, ASN A:209, LEU A:229, TYR A:159	HIS A:160, HIS A:164.

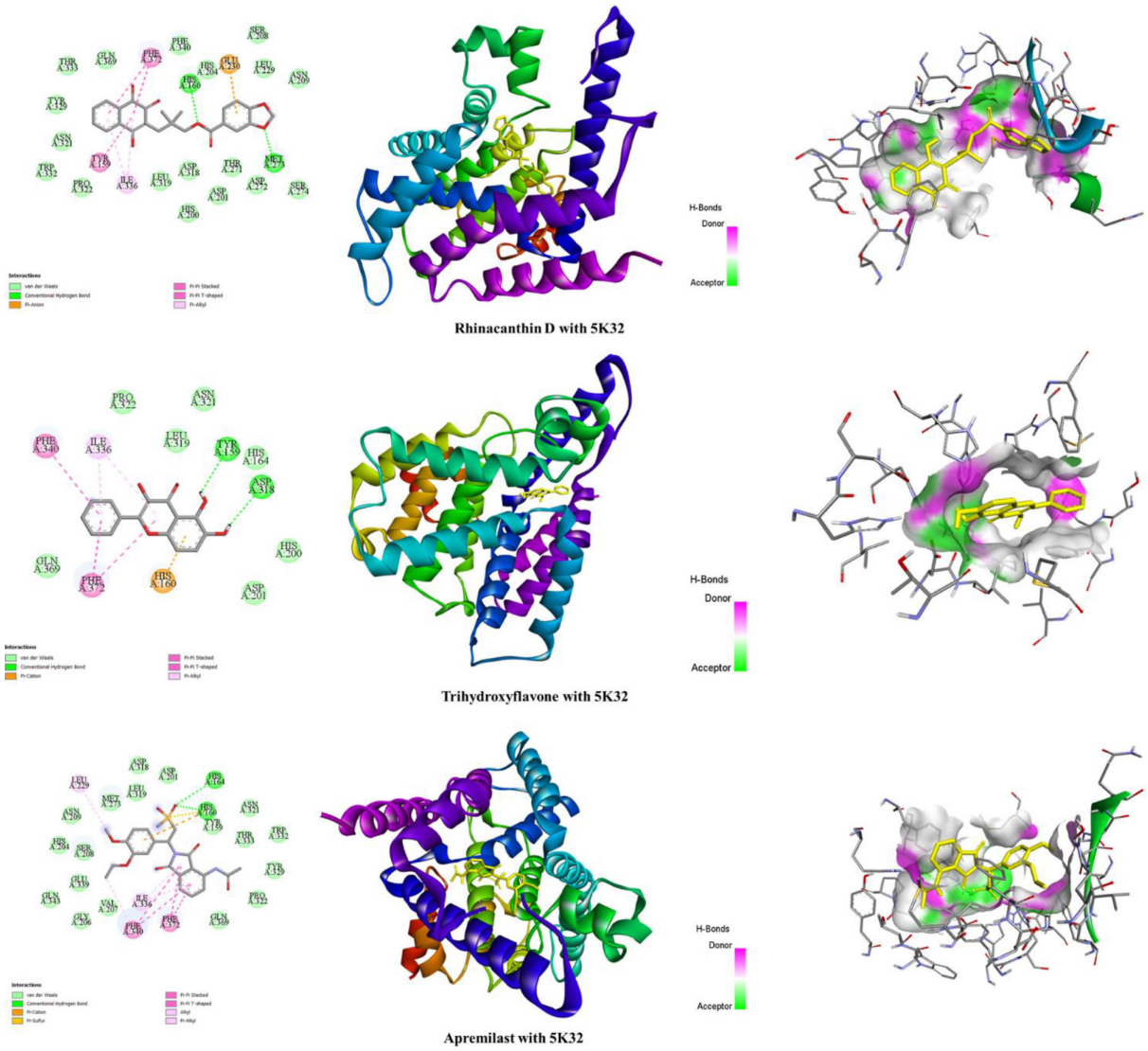

Figure 1. The figure illustrates 2D and 3D binding interactions of rhinacanthin D, trihydroxyflavone, and apremilast with the 5K32 protein.

Table 5. Docking scores, amino acid interactions, and hydrogen bonds of rhinacanthin D, trihydroxyflavone, and deucravacitinib with 4GIH

S. No	Compound	Docking Score	Amino Acid Interaction	Conventional Hydrogen Interaction
1	Rhinacanthin D	-9.3	ALA A:928, VAL A:911, LEU A:903, LEU A:1030, ILE A:960, MET A:978, VAL A:981, TYR A:980, GLU A:979, GLU A:905, GLY A:904, GLY A:906, GLY A:984, GLY A:985, GLY A:1040, LYS A:930, ASP A:1041, ASP A:988, ASN A:1028, ARG A:1027.	A:1027, ASP A:1041.
2	Trihydroxyflavone	-8.6	ALA A:928, VAL A:911, LEU A:903, LEU A:1030, ILE A:960, MET A:978, VAL A:981, TYR A:980, GLU A:979, GLU A:905, GLY A:904, GLY A:906, GLY A:984, GLY A:985, ASP A:1041, LYS A:930	VAL A:981.
3	Deucravacitinib	-8.0	ILE A:960, VAL A:911, LEU A:983, LEU A:1030, MET A:978, ASP A:1041, LYS A:930, LEU A:903, SER A:985, ASP A:988, ARG A:1027, ARG A:987, GLY A:904, GLY A:984, TYR A:980, VAL A:981, ARG A:901, GLY A:1040	LEU A:903.

Both phytoconstituents demonstrated strong interaction with the S1P1 receptor (3V2W) (Table 6, Figure 3), which is involved in the regulation of immune cell trafficking. Here, trihydroxyflavone (-9.1 kcal/mol) surpassed rhinacanthin D (-8.7 kcal/mol) and greatly outperformed Ponesimod's docking score of -6.0 kcal/mol. The data suggests possible involvement of the flavonoid in the control of lymphocyte egress leading to dampened systemic inflammation.

The docking data suggests that these phytochemicals could have multi-target effects by simultaneously modulating PDE4D, TYK2, and S1P1R, which are pivotal in psoriasis pathogenesis.

3.1 Molecular Dynamic Simulations of Tyk2, Lipid G and PDE4D Protein, in Complex with Compound Trihydroxyflavone and Rhinacanthin D

To assess the binding of two compounds, namely, compound trihydroxyflavone and rhinacanthin D with Tyk2, Lipid G and PDE4D protein, we conducted Molecular Dynamics (MD) simulations lasting 100 ns for 3 models (Figure 4) namely: Tyk2 protein - rhinacanthin D, lipid G protein - trihydroxyflavone and PDE4D protein - rhinacanthin D (as depicted in Figure 1). These simulations were subject to analysis using a range of statistical parameters,

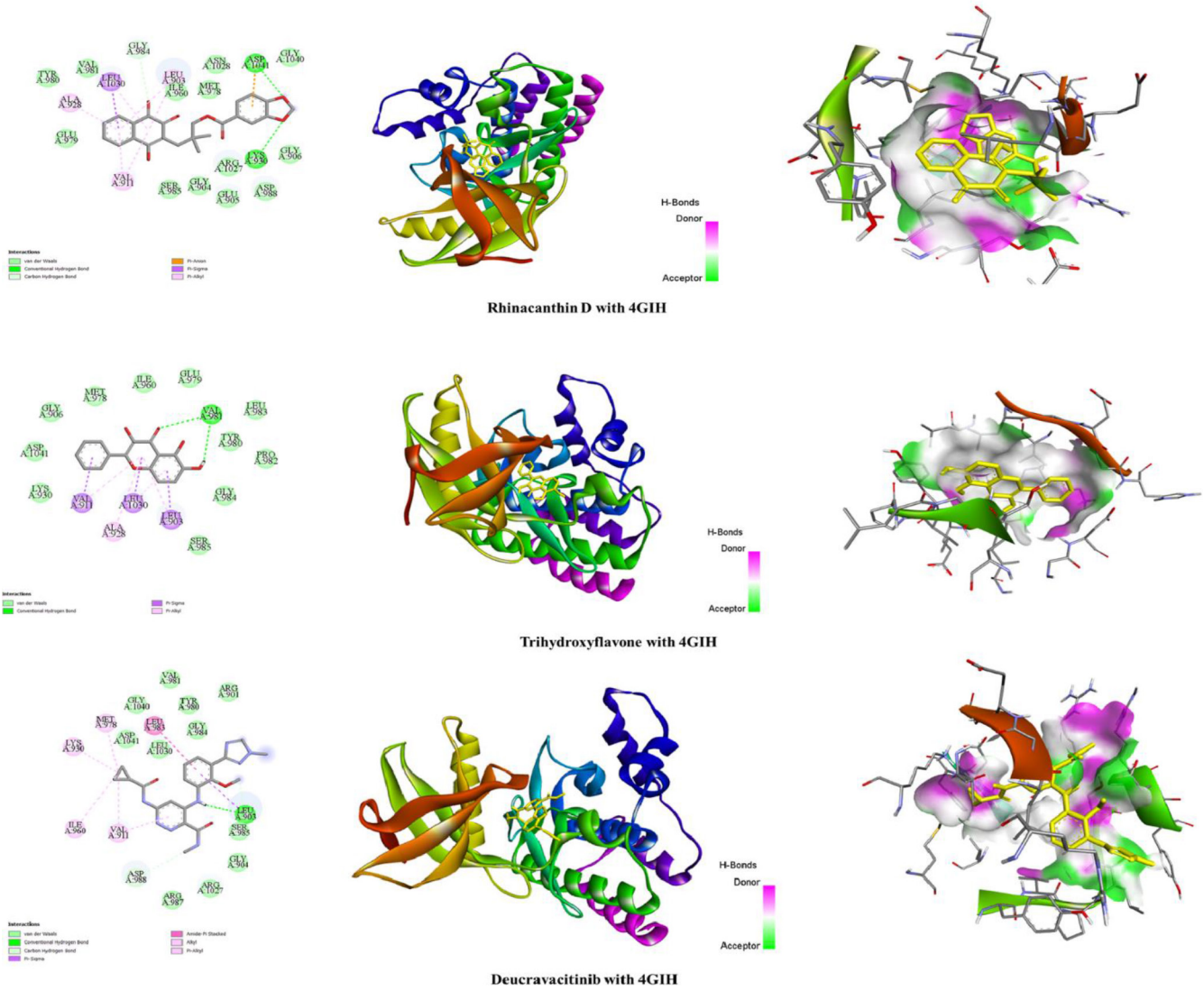

Figure 2. The figure illustrates 2D and 3D binding interactions of rhinacanthin D, trihydroxyflavone, and deucravacitinib with the 4GIH protein.

Table 6. Docking scores, amino acid interactions, and hydrogen bonds of rhinacanthin D, trihydroxyflavone, and ponesimod with 3V2W

S. No.	Compound	Docking Score	Amino Acid Interaction	Conventional Hydrogen Interaction
1	Rhinacanthin D	-8.7	LYS A:34, ASN A:101, GLU A:121, GLU A:294, SER A:105, TYR A:98, ARG A:120, THR A:109, GLY A:106, PHE A:125, TRP A:269, LEU A:128, LEU A:276, LEU A:272, LEU A:195, CYS A:206, ILE A:203, PHE A:210, MET A:124, LEU A:297, VAL A:194, LEU A:127.	LYS A:34
2	Trihydroxyflavone	-9.1	PHE A:125, TRP A:269, LEU A:128, LEU A:195, MET A:124, LEU A:297, GLU A:121, LEU A:276, LEU A:272, ASN A:101, GLU A:294, VAL A:194, TYR A:98.	-
3	Ponesimod	-6.0	LEU A:119, VAL A:126, ALA A:127, LEU A:172, LEU A:93, GLY A:122, TRP A:168, ASN A:86, SER A:123, LEU A:89, ALA A:126, VAL A:126, ALA A:127.	ASN A:86

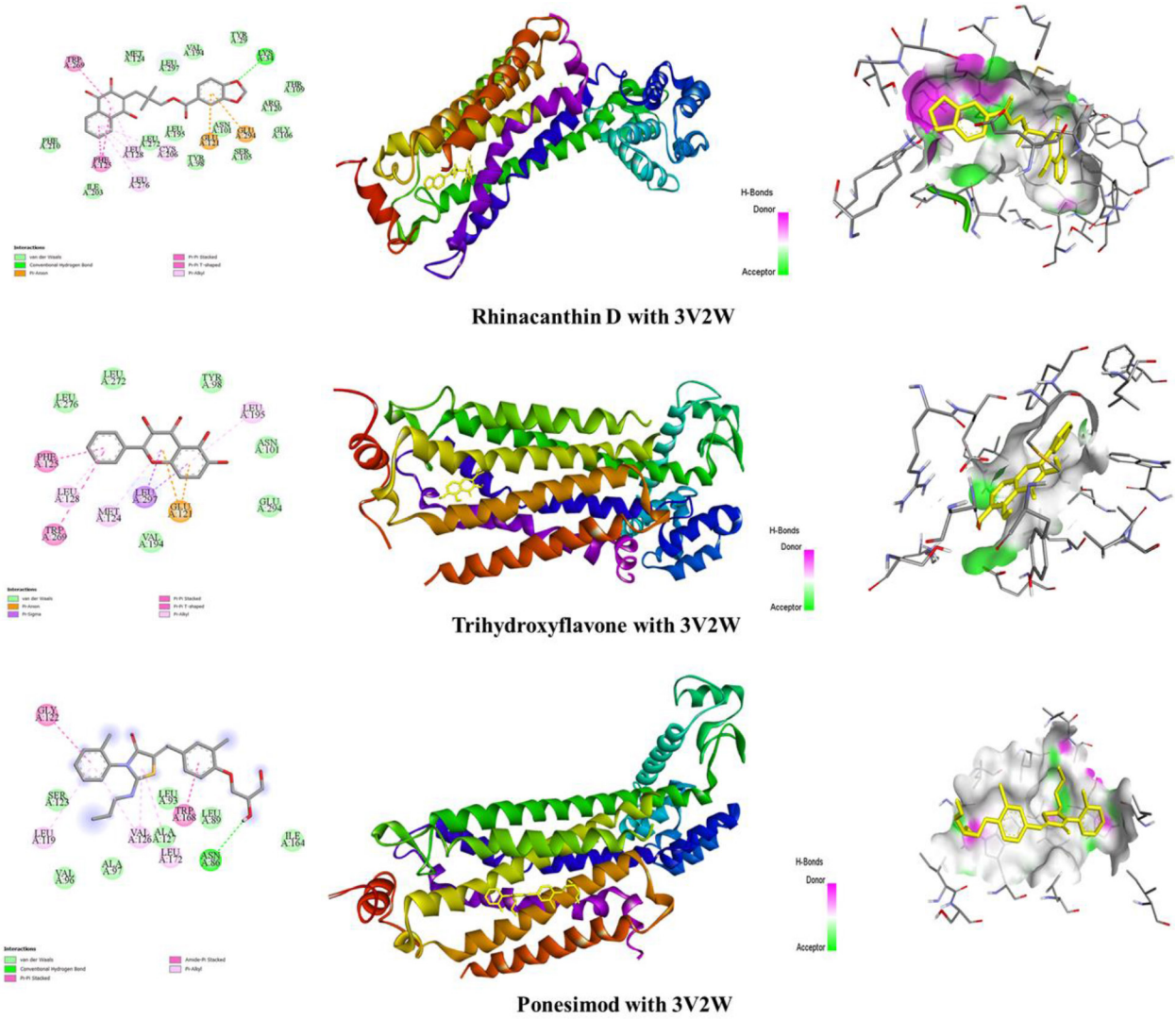

Figure 3. The figure illustrates 2D and 3D binding interactions of rhinacanthin D, trihydroxyflavone, and ponesimod with the 3V2W protein.

including Root-Mean-Square Deviation (RMSD), Root-Mean-Square Fluctuation (RMSF), hydrogen bond interactions, and their respective percentage occupancies over the simulation period.

3.2 RMSD Analysis

The RMSD analysis was performed to evaluate the structural stability of the ligand-protein complexes throughout the 100 ns molecular dynamics simulation. The RMSD plot shows how the structures of 3 complexes change over time: Rhinacanthin D-PDE4D, trihydroxyflavone–Lipid G, and rhinacanthin D-Tyk2 (Figure 5). The trihydroxyflavone-Lipid G complex (red curve) had the highest RMSD values of the three systems. It rose quickly in the first 10 ns and stayed stable around 0.90-1.10 nm for the rest of the simulation. This means that the protein-ligand complex may have a lot of conformational flexibility or even local rearrangements, even though the system stayed stable after equilibration. The rhinacanthin D-PDE4D (green curve) and rhinacanthin D-Tyk2 (blue curve) complexes, on the other hand, had much lower RMSD values, which stayed between 0.15 and 0.20 nm. These numbers show that the structure didn't change much from the original shape, which means that the structure was very stable and the ligand-protein interactions were very strong during the entire simulation. The RMSD profiles of the rhinacanthin D-bound complexes are fairly stable, which suggests that these ligands consistently interact with their target proteins. This may help make the binding more stable. The rhinacanthin D-Tyk2 complex behaved a little more consistently than the PDE4D complex, which suggests that it fits a little better and doesn't change shape as much. In general, the RMSD trends show that rhinacanthin D has good dynamic stability with both PDE4D and Tyk2 proteins.

The ligands were evaluated using the ligand RMSD analysis to examine the stability and binding patterns of the ligands in their protein binding sites during the entire MD simulation of 100 ns. The rmsd profile gives one an idea of how stable is each ligand when bound to its target protein. The rhinacanthin D-PDE4D structure (green trace) showed intermediate deviations of the ligand, which went across 0.22 nm after 20 ns, establishing to a constantly low value afterwards with low deviation. This suggests that rhinacanthin D underwent some slight positional adaptations inside the PDE4D binding pocket, but with overall similar interaction during the course of the simulation (Figure 6). The RMSD of trihydroxyflavone-lipid G complex (red line) were relatively low and were in the range of 0.07-0.12 nm after system equilibration. Limited

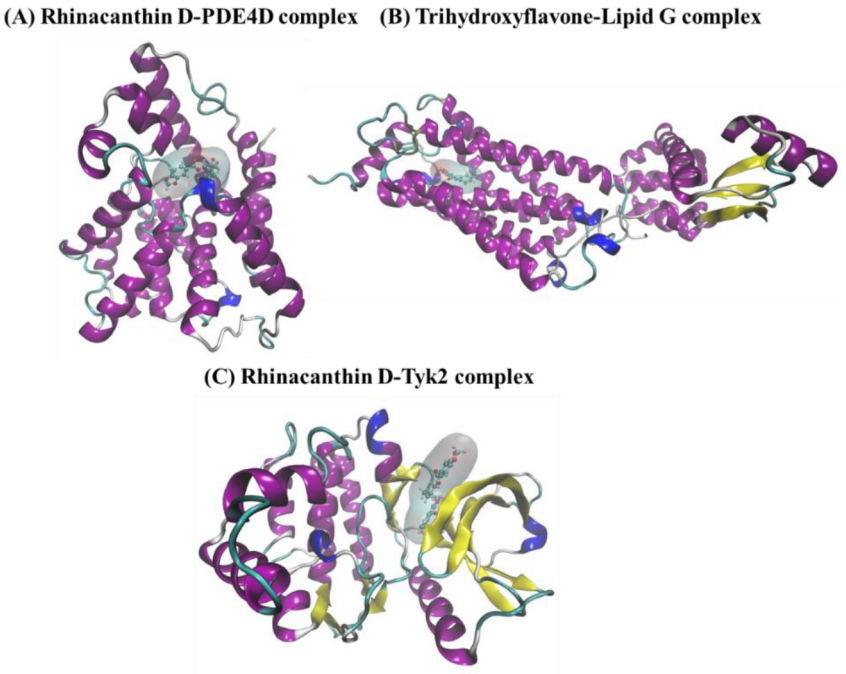

Figure 4. Graphical representation of protein-ligand complexes: **(A).** Rhinacanthin D-PDE4D protein; (B). Trihydroxyflavone-lipid G protein **(C).** Rhinacanthin D-Tyk2 protein.

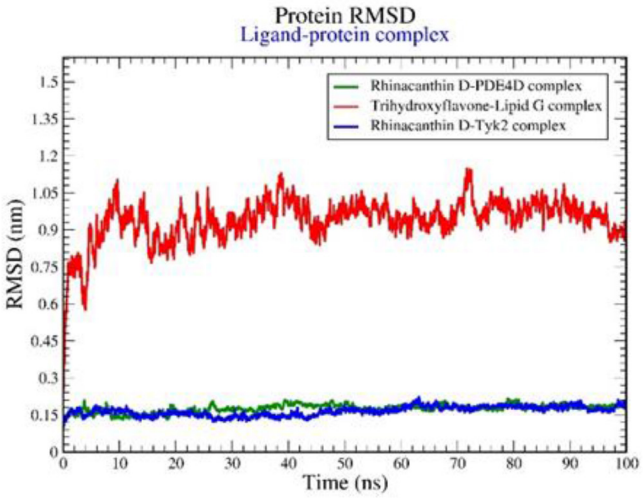

Figure 5. Graphical representation of the plots showing protein RMSD (nm) versus time (100 ns) for **(A).** Rhinacanthin D-PDE4D protein (green); **(B).** Trihydroxyflavone-lipid G protein (Red); **(C).** Rhinacanthin D-Tyk2 protein (blue).

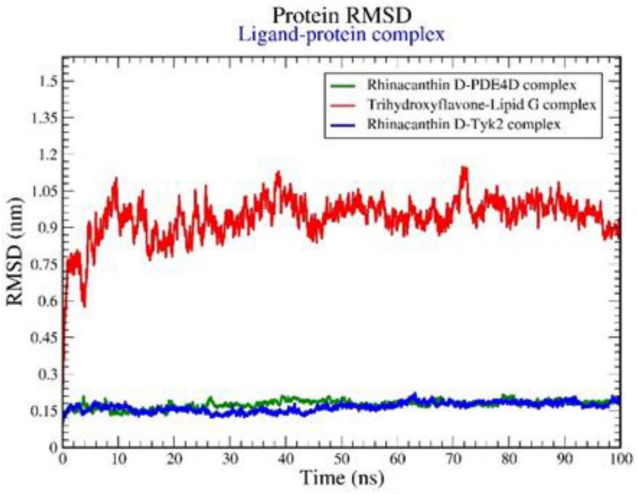

Figure 6. Graphical representation of the plots showing ligand RMSD (nm) versus time (100 ns) for **(A).** Rhinacanthin D-PDE4D protein (green); **(B).** Trihydroxyflavone-lipid G protein (red); **(C).** Rhinacanthin D-Tyk2 protein (blue).

fluctuations indicate that the ligand remained in a stable binding pose, which implies strong and stable interactions with the lipid G protein during the whole trajectory. The ligand RMSD profile of the rhinacanthin D-Tyk2 complex (blue curve) was the most stationary compared to the two other systems. Throughout the first 65 ns, the RMSD values stayed less than 0.10 nm and a slight increase was observed at 0.13 nm during the remaining period. This small shift further implies that rhinacanthin D would have stayed fit in its top-scored orientation within the Tyk2 binding pocket, indicating good position and shape complementarity between ligand and receptor. Overall, all 3 ligands exhibited acceptable RMSD values, reinforcing their stable binding over the simulation period. However, the rhinacanthin D-Tyk2 complex exhibited the highest stability, indicating that rhinacanthin D has strong potential as a Tyk2 inhibitor. Meanwhile, trihydroxyflavone also demonstrated excellent retention in the binding cavity of lipid G, supporting its potential bioactivity.

3.3 RMSF Analysis

The Root Mean Square Fluctuation (RMSF) analysis was performed to assess the flexibility of individual amino acid residues in the protein-ligand complexes over the course of the 100 ns molecular dynamics simulation. RMSF provides insight into the dynamic behavior of specific regions of the protein, particularly highlighting flexible loops or regions involved in ligand binding. The trihydroxyflavone-lipid G complex (red line) exhibited higher fluctuations in multiple regions, particularly at the N- and C-terminal ends, with RMSF values peaking around 0.80 nm. Several central regions also displayed notable flexibility, which may reflect inherent loop mobility or allosteric site movement within the protein (Figure 7). Despite these fluctuations, the core binding region appears to remain moderately stable. The Rhinacanthin D-PDE4D complex (green trace) demonstrated a more restricted RMSF profile, with fluctuations largely remaining below 0.30 nm. The highest peak was observed around residue 400, suggesting some degree of local flexibility, possibly at a loop or solvent-exposed region. Overall, this profile suggests that rhinacanthin D binding stabilizes most regions of the PDE4D protein structure. In contrast, the rhinacanthin D-Tyk2 complex (blue curve) showed the lowest RMSF values among the three complexes. The majority of residues fluctuated below 0.20 nm, indicating a highly rigid and stable protein conformation throughout the simulation. Only the terminal regions showed minor fluctuations, which is expected due to their solvent exposure and structural flexibility. Collectively, the RMSF analysis reveals that

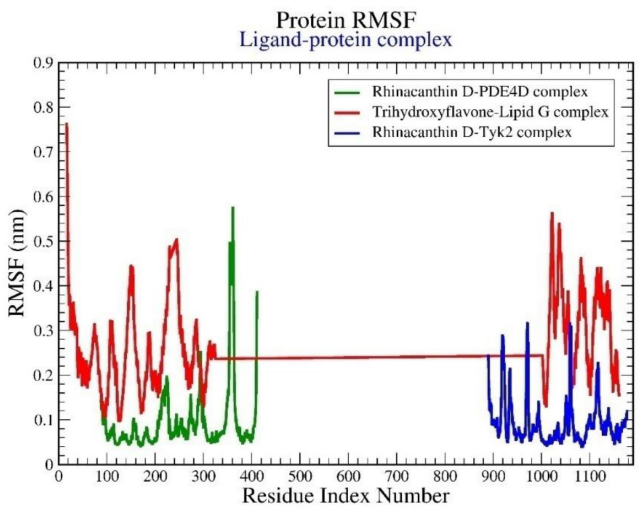

Figure 7. Graphical representation of the plots showing the protein RMSF (nm) versus residue index number of protein for **(A).** Rhinacanthin D-PDE4D protein (green); **(B).** Trihydroxyflavone-lipid G protein (red); **(C).** Rhinacanthin D-Tyk2 protein (blue).

rhinacanthin D contributes to enhanced structural stability in both PDE4D and Tyk2 protein targets, particularly in comparison to trihydroxyflavone's interaction with lipid G. These findings align well with RMSD results and support the inference that rhinacanthin D forms more stable and less dynamic complexes, especially with Tyk2.

3.4 H-bond Interaction

Hydrogen bond formation plays a pivotal role in stabilizing ligand-protein interactions during molecular dynamics simulations. The number and persistence of hydrogen bonds throughout the simulation provide insights into the strength and stability of the binding complex. For the rhinacanthin D-PDE4D complex, the number of hydrogen bonds fluctuated predominantly between 1 to 4 throughout the 100 ns simulation, with occasional spikes up to 5 hydrogen bonds (Figure 8). The consistency in maintaining at least 2 hydrogen bonds during the majority of the simulation period indicates a stable interaction pattern between rhinacanthin D and PDE4D. However, intermittent fluctuations suggest moderate dynamic behavior in the binding site environment. In the case of the trihydroxyflavone-lipid G complex, the number of hydrogen bonds ranged mainly from 1-4, similar to the rhinacanthin D-PDE4D complex. However, the

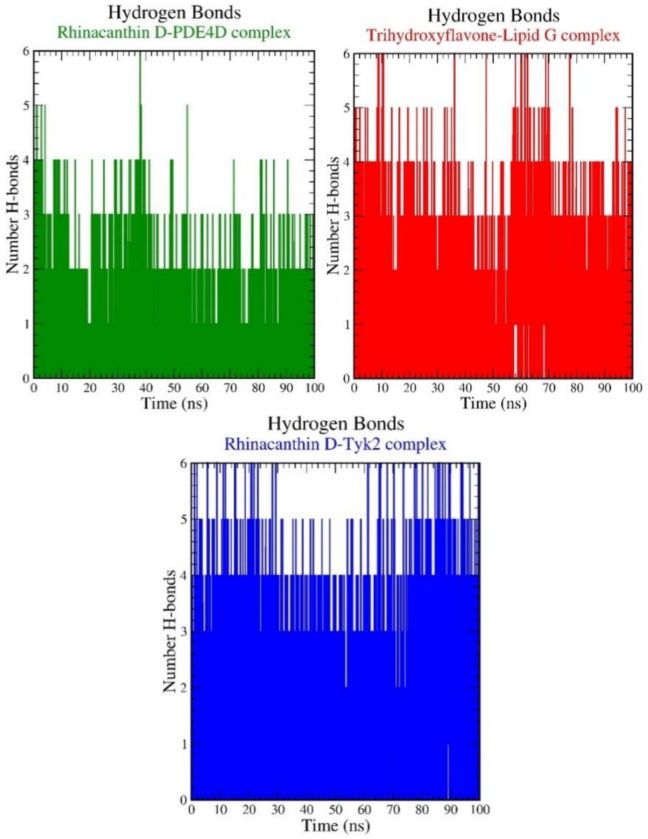

Figure 8. Pictorial representation of the number of h-bond contacts formed by ligands **(A).** rhinacanthin D-PDE4D protein (green); **(B)**. Trihydroxyflavone-lipid G protein (red); **(C).** Rhinacanthin D-Tyk2 protein (blue).

frequency of bond breakage was comparatively higher, with a few frames showing a reduction to zero hydrogen bonds. This suggests that although trihydroxyflavone forms stable interactions for certain periods, the overall binding may be relatively less stable or more transient compared to the other complexes. The rhinacanthin D-Tyk2 complex demonstrated the most stable hydrogen bonding pattern among all three complexes. The system consistently maintained 3-5 hydrogen bonds for the majority of the simulation period, rarely dropping below 3. This persistent interaction profile indicates a strong and stable binding of rhinacanthin D within the active site of Tyk2. The higher frequency and continuity of hydrogen bonds imply a tighter ligand accommodation and potentially stronger affinity. In summary, rhinacanthin D exhibits more robust and consistent hydrogen bonding patterns, especially with the Tyk2 target, indicating a highly stable complex formation. In contrast, trihydroxyflavone shows more

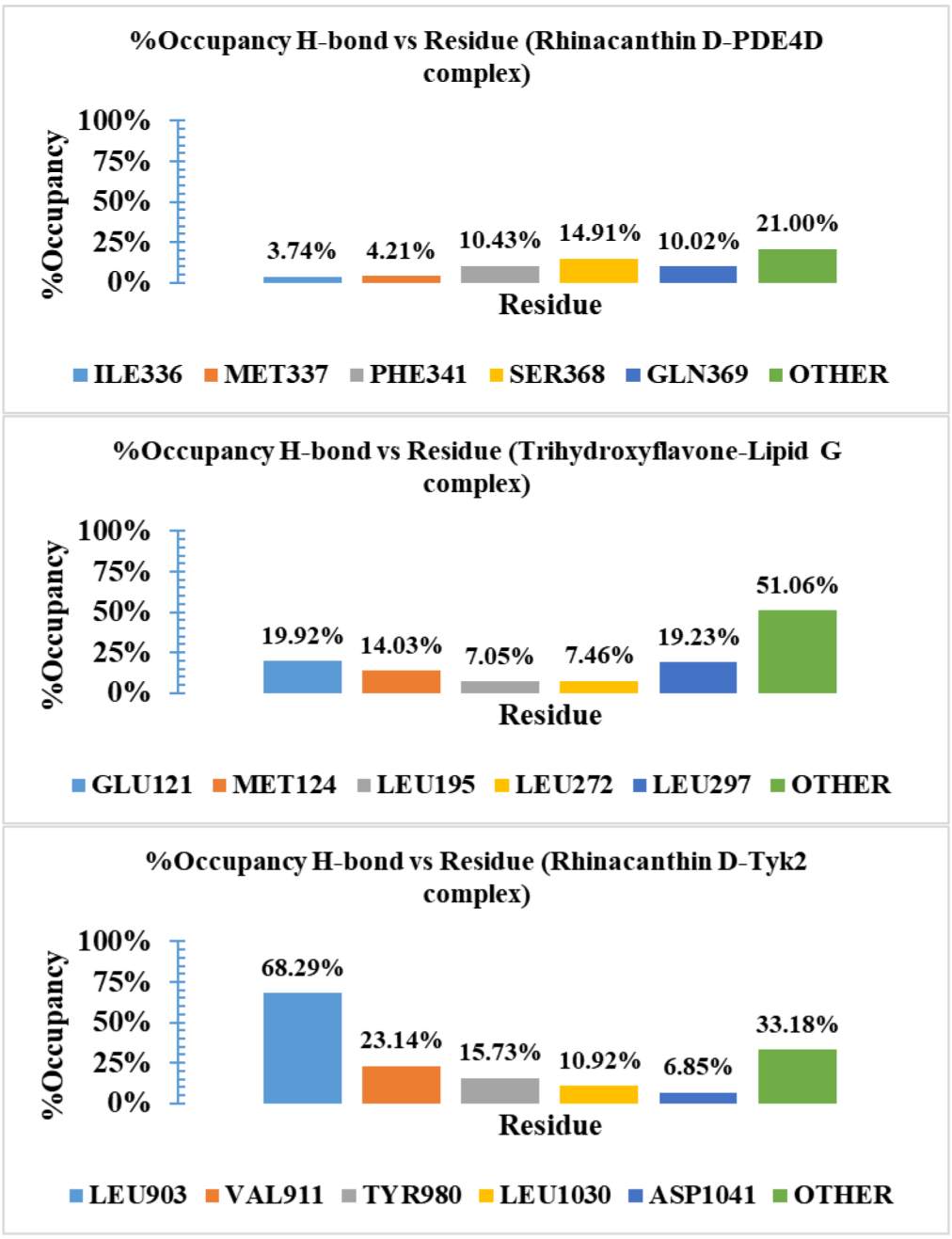

Figure 9. Histogram representation of % occupancies of the h-bond protein-ligand contacts of **(A).** Rhinacanthin D-PDE4D protein (green); **(B).** Trihydroxyflavone-lipid G protein (red); **(C).** Rhinacanthin D-Tyk2 protein (blue).

fluctuating behavior, which might correlate with less favorable or more flexible binding interactions. These results support the hypothesis that rhinacanthin D could serve as a more potent ligand with better structural stability in complex with its target protein.

Figure 9 displays a histogram representing the percentage occupancies of hydrogen bond contacts formed by different ligands. Occupancy analysis further confirmed the interaction stability: Rhinacanthin D-PDE4D: Residues SER368 (14.91%), GLN369 (10.02%), and PHE341 (10.43%) showed significant H-bond occupancy, supporting their roles in ligand anchoring. Trihydroxyflavone-lipid G: Residues GLU121 (19.92%) and LEU297 (19.23%) contributed notably to hydrogen bonding, though with greater diversity in interacting residues. Rhinacanthin D-Tyk2:

Table 7. MMGBSA ΔG binding energy calculations for **(A)** Rhinacanthin D-PDE4D protein (green) **(B)** Trihydroxyflavone-lipid G protein (red) **(C)** Rhinacanthin D-Tyk2 protein (blue)

Ligand-protein Complex	0 ns	50 ns	100 ns	Average
Rhinacanthin D-PDE4D complex	-48.9	-61.3	-35.2	-48.47
Trihydroxyflavone-lipid G complex	-51.5	-85.1	-35.4	-57.33
Rhinacanthin D-Tyk2 complex	-56.1	-67.9	-78.7	-67.57

LEU903 dominated with 68.29% occupancy, followed by VAL911 (23.14%) and TYR980 (15.73%), indicating highly focused and stable interactions.

3.4.1 MMGBSA Calculations

To gain insight into the binding free energy and interaction strength of the ligand-protein complexes, MM/GBSA (Molecular Mechanics/Generalized Born Surface Area) calculations were performed at 3 time intervals-0 ns, 50 ns, and 100 ns-during the 100 ns molecular dynamics simulations. The average binding free energy (ΔG) over these time points was used to evaluate the stability and affinity of the ligands toward their respective targets. Among the 3 systems analyzed, the rhinacanthin D-Tyk2 complex demonstrated the most favorable binding affinity, with an average ΔG of -67.57 kcal/mol. This strong interaction was consistent across all sampled frames, with the lowest binding energy observed at 100 ns (-78.7 kcal/mol), indicating improved ligand accommodation and enhanced interaction over time. The trihydroxyflavone-lipid G complex also showed notable binding strength, with an average ΔG of -57.33 kcal/mol. A significant binding energy of -85.1 kcal/mol at 50 ns suggests transient periods of enhanced interaction, although a decline at 100 ns (-35.4 kcal/mol) implies some instability or conformational rearrangement during the later stage of the simulation. In comparison, the rhinacanthin D-PDE4D complex exhibited relatively weaker binding, with an average ΔG of -48.47 kcal/mol. The energy values fluctuated moderately throughout the simulation, suggesting less consistent interaction dynamics with the PDE4D binding site. Overall, MM/GBSA results reinforce the molecular stability findings

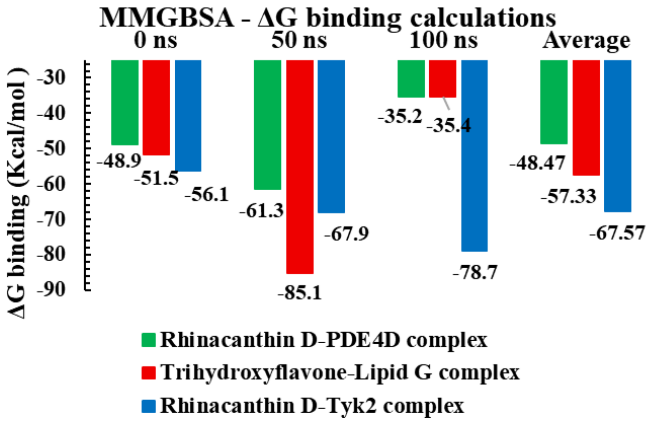

Figure 10. MMGBSA ΔG binding energy calculations **(A).** Rhinacanthin D-PDE4D protein (green); **(B).** Trihydroxyflavone-lipid G protein (red); **(C).** Rhinacanthin D-Tyk2 protein (blue).

observed in hydrogen bonding and RMSD analyses (Table 7, Figure 10). The rhinacanthin D-Tyk2 complex emerges as the most promising interaction model, supported by both high binding affinity and stable hydrogen bond formation. These findings suggest that rhinacanthin D may serve as a potent inhibitor of Tyk2, with potential therapeutic relevance pending further experimental validation.

4. SASA

The Solvent-Accessible Surface Area (SASA) analysis over a 100 ns molecular dynamics simulation revealed that all three ligand-protein complexes attained structural stability with minimal fluctuations after initial equilibration. Among them, the trihydroxyflavone-lipid G complex exhibited the highest average SASA (245 nm^2), indicating greater solvent exposure, possibly due to a less compact binding interface or the larger size of lipid G. In contrast, the rhinacanthin D-Tyk2 complex showed the lowest SASA (~150 nm^2), reflecting a more tightly packed and stable conformation, likely due to a snug ligand fit within the Tyk2 binding pocket. The rhinacanthin D-PDE4D complex maintained an intermediate SASA (~165 nm^2), suggesting moderate solvent accessibility. The relatively narrow fluctuation ranges in all complexes indicate the absence of significant structural deviations, supporting the conformational stability of each system (Figure 11). These differences in SASA profiles provide insights into the compactness and binding interactions of the

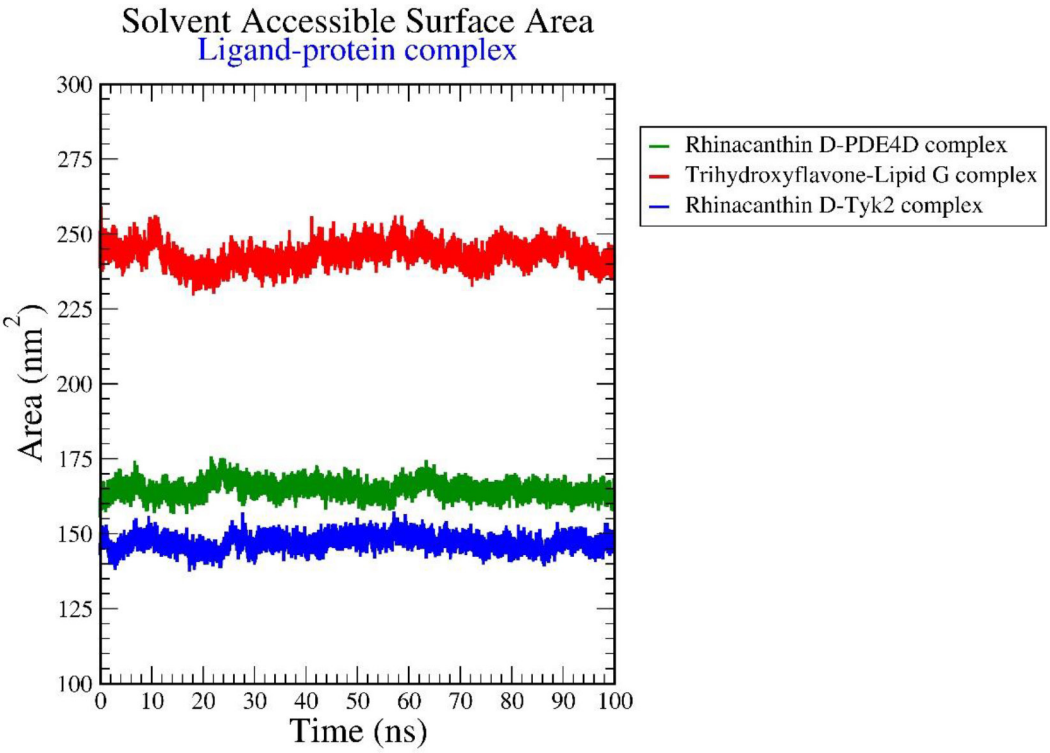

Figure 11. SASA calculation **(A).** Rhinacanthin D-PDE4D protein (green); **(B).** Trihydroxyflavone-lipid G protein (red); **(C).** Rhinacanthin D-Tyk2 protein (blue).

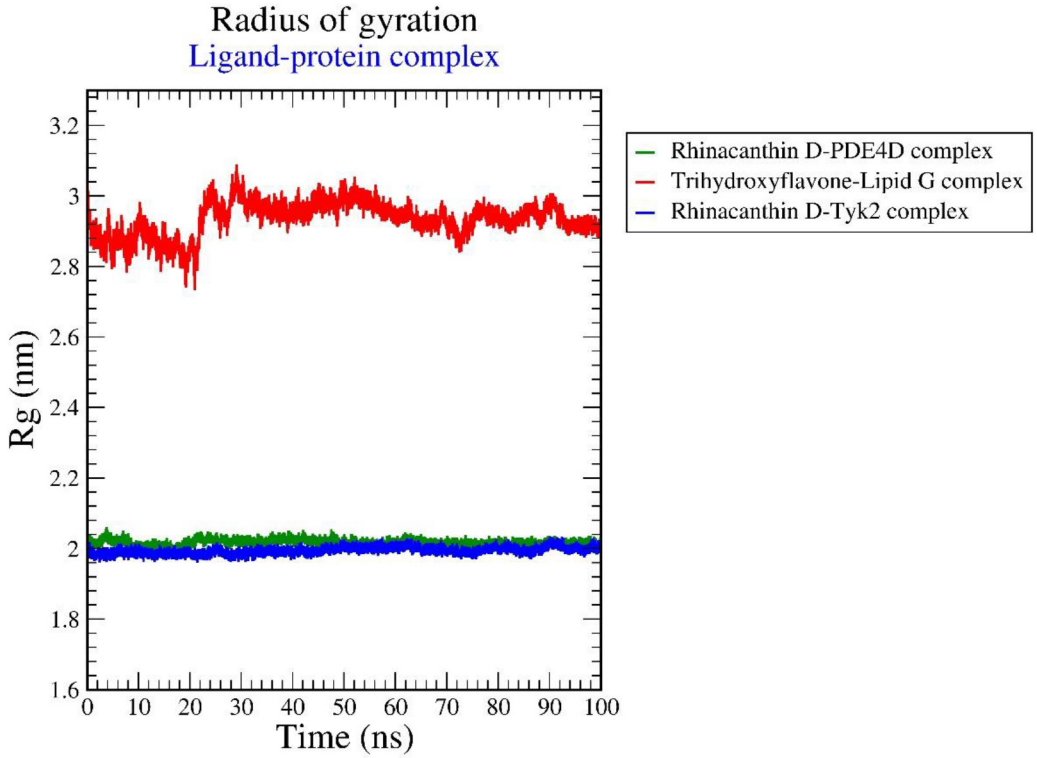

Figure 12. Radius of gyration of calculation **(A).** Rhinacanthin D-PDE4D protein (green); **(B).** Trihydroxyflavone-lipid G protein (red); **(C).** Rhinacanthin D-Tyk2 protein (blue).

ligands, which can be valuable for guiding further optimisation in drug design.

5. Radius of Gyration

The Radius of gyration (Rg) analysis was performed to evaluate the compactness and structural stability of the ligand-protein complexes over a 100 ns molecular dynamics simulation. As shown in the plot, all 3 complexes maintained relatively stable Rg values throughout the simulation period, indicating the absence of major conformational changes. The rhinacanthin D-Tyk2 (blue) and rhinacanthin D-PDE4D (green) complexes exhibited nearly identical Rg values, averaging around 2.0 nm with minimal fluctuations, suggesting that both protein systems retained a compact and well-folded structure during ligand binding. In contrast, the trihydroxyflavone-lipid G complex (red) displayed a significantly higher Rg, ranging between 2.85 to 3.05 nm. This elevated value reflects a comparatively more extended structure, which may be attributed to the inherent size or flexible domains of the lipid G protein. The slight increase and stabilisation of Rg after 30 ns further suggest some initial conformational adjustment upon ligand accommodation, followed by a stable configuration for the remainder of the simulation. Overall, the low variability in Rg for all complexes confirms that ligand binding did not induce global unfolding or destabilisation. The relatively compact Rg profiles of the rhinacanthin D-bound systems imply stronger and more stable interactions (Figure 12), which may contribute to enhanced binding efficiency. Meanwhile, the broader structure observed in the lipid G complex may require further analysis to assess the impact on ligand affinity and target specificity. These findings support the conformational integrity and suitability of the simulated complexes for further drug development studies.

6. Conclusion

This research presents strong *in silico* evidence for the efficacy of *R. nasutus* (rhinacanthin D) and *S. nigrum* (trihydroxyflavone) bioactive compounds as multi-targeted anti-psoriatic drugs. Molecular docking demonstrated that rhinacanthin D had better binding affinities to primary psoriasis-associated targets- PDE4D (-9.5 kcal/mol), TYK2 (-9.3 kcal/mol), and S1P1R (-8.7 kcal/mol)- compared to current drugs such as Apremilast, Deucravacitinib, and Ponesimod. Trihydroxyflavone also demonstrated strong interactions, particularly with S1P1R (-9.1 kcal/mol), suggesting its role in modulating immune cell trafficking. The pharmacokinetic profiles of these compounds, assessed *via* SwissADME, confirmed favorable drug-likeness and oral bioavailability, adhering to Lipinski's, Veber's, and Ghose's rules. Molecular dynamics simulations (100 ns) further validated the stability of the ligand-protein complexes. Rhinacanthin D-TYK2 had the greatest stability (RMSD ~0.15-0.20 nm, RMSF <0.20 nm, and regular 3-5 hydrogen bonds) as well as the most favorable binding free energy (ΔG = -67.57 kcal/mol) and was predicted to be a potent inhibitor of TYK2. Rhinacanthin D-PDE4D complex was moderately stable (ΔG = -48.47 kcal/mol), while trihydroxyflavone-lipid G had increased conformational flexibility (ΔG = -57.33 kcal/mol). SASA and radius of gyration studies supported the compactness and structural stability of these complexes, especially for rhinacanthin D-bound systems. These data validate the ethnomedicinal utilization of *R. nasutus* and *S. nigrum* against inflammatory skin conditions such as psoriasis and identify rhinacanthin D and trihydroxyflavone as potential lead compounds. Their multi-target activities on PDE4D, TYK2, and S1P1R indicate a synergistic strategy to regulate the multifaceted inflammatory pathways in psoriasis. Nonetheless, as computational predictions cannot fully account for biological complexity, further *in vitro* and *in vivo* studies are required to validate efficacy, safety, and therapeutic applicability.

7. Author Contribution

Vijayalakshmi A conceptualised the study, provided scientific guidance throughout the research, and critically reviewed the manuscript. Vaheeda Rahman contributed to structuring the manuscript, refining the flow of content, and ensuring coherence in scientific presentation. All authors have read and agreed to the published version of the manuscript.

8. References

1. Campanati A, Marani A, Martina E, Diotallevi F, Radi G, Offidani A. Psoriasis as an immune-mediated and inflammatory systemic disease: From pathophysiology to novel therapeutic approaches. Biomedicines. 2021; 9(11):1511. https://doi.org/10.3390/biomedicines9111511
2. Li L, Liu J, Lu J, Wu J, Zhang X, Ma T, *et al*. Interventions in cytokine signaling: Novel horizons for psoriasis treatment. Front Immunol. 2025; 16:1573905. https://doi.org/10.3389/fimmu.2025.1573905
3. Silvagni E, Missiroli S, Perrone M, Patergnani S, Boncompagni C, Bortoluzzi A, *et al.* From bed to bench and back: TNF-α, IL-23/IL-17A, and JAK-dependent inflammation in the pathogenesis of psoriatic synovitis. Front Pharmacol. 2021; 12:672515. https://doi.org/10.3389/fphar.2021.672515
4. Guo J, Zhang H, Lin W, Lu L, Su J, Chen X. Signaling pathways and targeted therapies for psoriasis. Signal Transduct Target Ther. 2023; 8(437). https://doi.org/10.1038/s41392-023-01655-6
5. Shamsi A, Khan MS, Altwaijry N, Hassan N, Shahwan M, Yadav DK. Targeting PDE4A for therapeutic potential: Exploiting drug repurposing approach through virtual screening and molecular dynamics. J Biomol Struct Dyn. 2023; 43(11):5423-5435. https://doi.org/10.1080/07391102.2024.2308764
6. Zhou Y, Li X, Shen R, Wang X, Zhang F, Liu S, *et al*. Novel small molecule tyrosine kinase 2 pseudokinase ligands block cytokine-induced TYK2-mediated signaling pathways. Front Immunol. 2022; 13:884399. https://doi.org/10.3389/fimmu.2022.884399
7. Liu S, Paknejad N, Zhu L, Kihara Y, Ray M, Chun J, *et al*. Differential activation mechanisms of lipid GPCRs by lysophosphatidic acid and sphingosine 1-phosphate. Nat Commun. 2022; 13(731). https://doi.org/10.1038/s41467-022-28417-2
8. Ayan G, Ribeiro A, Macit B, Proft F. Pharmacologic treatment strategies in psoriatic arthritis. Clin Ther. 2023; 45(9):826-840. https://doi.org/10.1016/j.clinthera.2023.05.010
9. Saising J, Maneenoon K, Sakulkeo O, Limsuwan S, Gotz F, Voravuthikunchai SP, *et al*. Ethnomedicinal plants in herbal remedies used for treatment of skin diseases by traditional healers in Songkhla province, Thailand. Plants. 2022; 11(7):880. https://doi.org/10.3390/plants11070880
10. Tsioutsiou EE, Amountzias V, Vontzalidou A, Dina E, Stevanovic ZD, Cheilari A, *et al*. Medicinal plants used traditionally for skin related problems in the south Balkan and east Mediterranean region- a review. Front Pharmacol. 2022; 13:936047. https://doi.org/10.3389/fphar.2022.936047
11. Choedchutirakul N, Panthong S, Sakpakdeejaroen I, Thongdeeying P, Taingthum A, Bunpean A. *In vitro* anti-inflammatory and anti-allergenic effects of Thai herbal formula and its isolates, Rhinacanthin-C and Rhinacanthin-N in RBL-2H3 cells and RAW264.7 macrophages. Trop J Nat Prod Res. 2024; 8(11). https://doi.org/10.26538/tjnpr/v8i11.10
12. Hussain W, Amir A, Rasool N. Computer-aided study of selective flavonoids against chikungunya virus replication using molecular docking and DFT-based approach. Struct Chem. 2020; 31:1363-1374. https://doi.org/10.1007/s11224-020-01507-x
13. Nguyen PT, Tran Huynh QD, Nguyen MD. Isolation and purification of sinensetin, and *in silico* screening of phytochemicals from *Orthosiphon aristatus* (Blume) Miq. For anti-breast cancer activity. Nat Prod Res. 2025. https://doi.org/10.1080/14786419.2025.2495169
14. Thuong SD, Anh MTH, Phuong NV, Mau CH, Quan NH, Cong NT, *et al*. Chemical constituents and α-glucosidase inhibitory activities of the leaves of *Embelia parviflora in vitro* and *in silico* studies. Life. 2025; 15(5):680. https://doi.org/10.3390/life15050680
15. Priya K, Manandhar S, Sankhe R, Setty MM, Babu UV, Pai SR. Structure based virtual docking and molecular dynamics guided identification of potential phytoconstituents from traditionally used female antifertility plant. Pharm Sci. 2021; 28(2):285-294.
16. Milenkovic A, Aleksovski S, Miteva K, Milenkovic L, Stanojevic J, Nikolic G, *et al.* The effect of extraction technique on the yield, extraction kinetics and antioxidant activity of black pepper (*Piper nigrum* L.) ethanolic extracts. Horticulturae. 2025; 11(2):125. https://doi.org/10.3390/horticulturae11020125
17. Hamidon NH, Dona ACT, Zin NNINM, Nordin NI, Sulaiman SF, Abu-Bakar N. Bioassay-guided fractionation of acetone and methanol extracts of *Quercus infectoria* galls with antimalarial properties. Trop Life Sci Res. 2024; 35(2):167-185. https://doi.org/10.21315/tlsr2024.35.2.8
18. Tshiluka NR, Mbedzi DT, Bvumbi MV, Moleele SSM. *In vitro* αglucosidase inhibition, cytotoxicity, SAR, Swiss ADME prediction and molecular docking study of new Nsubstituted hydantoin derivatives. Chem Open. 2025; 14(4):e202400119. https://doi.org/10.1002/open.202400119
19. Sivakumar M, Roshni J, Ahmad SF, Attia SM, Ramasamy M, Ahmed SSSJ. Fused pyrido[3,4-d]pyrimidine moiety with phthalazinone ring accelerate dual inhibition of PARP1 and CDK4 in triple-negative breast cancer: A hybrid design with computational investigation through molecular modeling and quantum mechanics. J Mol Model. 2025; 31(181). https://doi.org/10.1007/s00894-025-06393-w
20. Swapna B, Kotha S, Selvaraj D, Ramachandra S, Acharya A. Probing the dark chemical matter against PDE4 for the management of psoriasis using *in silico*, *in vitro* and *in vivo* approach. Molecular Diversity.Springer. 2025; 29:3449-3464. https://doi.org/10.1007/s11030-025-11159-w

21. Mansouri P, Mansouri P, Najafipour S, Kouhpayeh SA, Farjadfar A, Behmard E. Comprehensive computational strategies for multitarget drug discovery in inflammatory bowel disease utilizing bioactive compounds. Sci Rep. 2025; 15(15542). https://doi.org/10.1038/s41598-025-98771-w
22. Biswasroy P, Pradhan D, Pradhan DK, Goyal A, Ghosh G, Rath G. *In silico*based molecular screening and evaluation of *in vivo* antiinflammatory activity of selected medicinal herbs for Psoriasis management. Research Journal of Pharmacy and Technology. 2025; 18(4):1743-1749. https://doi.org/10.52711/0974-360X.2025.00250
23. Rathor LS, Sahu D, Singh M, Singh D. *In silico* screening of phytochemicals as potential inhibitors of the JAK/STATs pathway in Psoriasis. Assay Drug Dev Technol. 2025; 23(2):100-113. https://doi.org/10.1089/adt.2024.087
24. Alizadeh AA, Jafari B, Dastmalchi S. Drug repurposing for identification of S1P1 agonists with potential application in multiple Sclerosis using *in silico* drug design approaches. Adv Pharm Bull. 2022; 13(1):113-122. PMID: 36721815. PMCID: PMC9871275. https://doi.org/10.34172/apb.2023.012
25. Tomar Y, Gorantla S, Singhvi G. Insight into the pivotal role of signaling pathways in psoriasis pathogenesis, potential therapeutic molecules and drug delivery approaches. Drug Discov Today. 2023; 28(2):103465. https://doi.org/10.1016/j.drudis.2022.103465
26. Achutha AS, Pushpa VL, Manoj KB. Comparative molecular docking studies of phytochemicals as Jak2 inhibitors using Autodock and Arguslab. Mater Today Proc. 2021; 41(Part 3):711-716. https://doi.org/10.1016/j.matpr.2020.05.661
27. Fatmawati Y, Sandrina S, Aina RN, Narulita E. Molecular docking analysis of seagrass (*Enhalus acoroides*) phytochemical compounds as an antidiabetic. J Biol Res-Boll Soc. 2022; 95(1). https://doi.org/10.4081/jbr.2022.10224
28. Zhou F, Yao H, Ma Z, Hu X. Investigating small molecule compounds targeting psoriasis based on cMAP database and molecular dynamics simulation. Skin Res Technol. 2023; 29(4):e13301. https://doi.org/10.1111/srt.13301
29. Sharma B, Purohit R. Structural insights into the lead identification of subtype selective PDE4B inhibitors from plant bioactive molecule analogues. J Mol Liq. 2023; 390(Part A):123039. https://doi.org/10.1016/j.molliq.2023.123039
30. Sardari E, Ebadi A, Asl NR. *In silico* repurposing of CNS drugs for multiple sclerosis. Mult Scler Relat Disord. 2023; 73:104622. https://doi.org/10.1016/j.msard.2023.104622